Communication

Formation of Sliver Defect in Ni-Based Single Crystal Superalloy

YAQI HUANG, JIAN SHEN, DONG WANG, GUANG XIE, YUZHANG LU, LANGHONG LOU, and JIAN ZHANG

The formation mechanism of sliver defect in Ni-based single crystal superalloy was investigated by X-ray computed tomography and electron backscattered diffraction. The origin of sliver due to the localized deformation of 1-2 dendrites near the mold wall was experimentally observed. The diverging boundary was the favorite position for sliver initiation. It was found that the deformation that induced sliver occurred in the mushy zone and was limited in the lower part of the dendrite. Thermal contraction forces played an important role in the formation of sliver. The dendrite deformation was attributed to the imbalanced force loaded on the dendrite.

https://doi.org/10.1007/s11661-019-05516-2

Nickel-based single crystal (SX) superalloys have been widely used in turbine blades for their exceptional high-temperature properties.[1,2] However, casting defects, such as stray grains,[3] freckle,[4] low angle boundary,[5] and sliver[6,7] are potential threats to the performance of the SX superalloys. At present, very limited information on the formation mechanism of sliver has been reported comparing to that of the other defects.

Sliver is observed as strip-like contrast in SX. It may extend along the directional solidification (DS) direction after formation.[6–8] Previous works confirmed that the origin of sliver is primarily associated with the deformation of dendrites in the mushy zone.[6,7] There have been numerous indirect observations of dendrite deformation in various materials.[9] The deformation has been linked to gravity,[10] elastic deformation,[11] γ' precipitation,[12] and solute field ahead of the solid-liquid interface.[13] During directional solidification, the dendrite deformation is possibly caused by: (I) Inter-dendritic fluid flow (convection) induced by alloying or processing conditions during solidification. The strong segregation in directional solidification of SX superalloy often results in the vertical fluid convection at a certain stage of solidification.[14] Both remelting at the neck of dendrite arms during coarsening, solute enhancement, or recalescence[15–17] and mechanical interactions[18,19] have been considered to cause the deformation or fragmentation of dendrites; (II) Thermal contraction during solidification. Aveson *et al.*[7] proposed that the sliver arose from the high stresses in the constricted channel due to different thermal contraction between mold and metal. Similar misorientation accumulated during DS has also been reported recently in a third generation SX superalloy.[20] Sun *et al.*[6] believed that the lateral sliver defects on the platform generated due to the high contraction stresses around the connections of platform and the SX body.

To date, the direct observation of dendrite deformation in the mushy zone is still lacking, and therefore, the exact reason leading to the deformation and the formation mechanism of sliver are still unclear. In this study, SX castings were produced, with a detailed X-ray computed tomography (XCT) and electron backscattered diffraction (EBSD) characterization. The formation mechanism has been explored based on the experimental evidence of dendrite deformation in the mushy zone.

The nominal composition of the superalloy PWA 1483 used in the experiments was (in wt pct): 0.05 C, 12.0 Cr, 9.0 Co, 4.0 W, 2.0 Mo, 3.4 Al, 4.0 Ti, and the balance in Ni. The SX casting with similar geometry of the airfoil section of a turbine blade was directionally solidified. The thickness of the cross section of the casting gradually increased from bottom to top in order to simulate the tip-down DS process of the real SX blade (Figure 1(a)). Ten mold clusters with six castings in each cluster were produced using the spiral grain selection method in a Bridgman furnace. The ceramic mold was preheated to 1500 °C. The master alloy was melted and poured into the preheated mold at 1500 °C and held at the temperature for 2 minutes before withdrawal. A constant withdrawal rate of 3 mm/min was used in all experiments. All castings were macro-etched (50 pct HCl-50 pct H_2O_2) after removing the ceramic shell and the SX starter. The samples with 10 mm in length and 1 mm × 1 mm in cross section were cut from the castings at the initial position of sliver for XCT (the lab-based Xradia Versa XRM-500 system) characterization as shown in Figure 1(b). The software of Avizofire 7.1 was employed to process and visualize the XCT results.[21,22] After that, the XCT sample was

YAQI HUANG is with the Superalloys Division, Institute of Metal Research, Chinese Academy of Sciences, Shenyang 110016, China and also with the School of Materials Science and Engineering, University of Science and Technology of China, Hefei 230026, China. JIAN SHEN, DONG WANG, GUANG XIE, YUZHANG LU, LANGHONG LOU, and JIAN ZHANG are with the Superalloys Division, Institute of Metal Research, Chinese Academy of Sciences. Contact e-mail: jianzhang@imr.ac.cn
Manuscript submitted July 22, 2019.
Article published online November 1, 2019

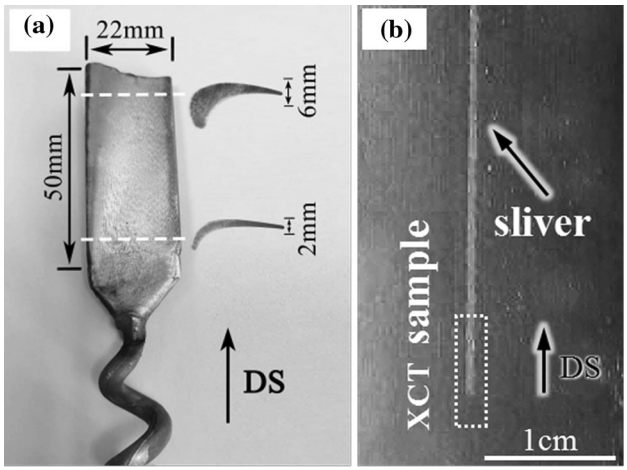

Fig. 1—(*a*) SX casting used in the experiments. (*b*) The typical morphology of sliver on surface of casting and schematic illustration of sampling.

carefully ground to the plane containing the deformed dendrites and then mechanically and electro-polished. The optical microscope (OM-IMc 5) and EBSD were then employed to characterize the microstructure and dendrite orientation, as well as the deformation. All data collected from EBSD were processed by the Oxford HKL Channel 5 software. The EBSD data were also quantified using the method described in Reference 7 to obtain the extent of bending and torsion angle of the dendrites.

9 castings containing a sliver were found among the sixty SX pieces after macro etching. Figure 1(b) shows the typical morphology of sliver on surface of the SX casting. The strip-like structure on matrix can be clearly observed, and the sliver defect extended along the DS direction to the top of the casting.

The XCT results of the sliver at its initiation position are exhibited in Figure 2. Dendrite structure in three sections with a distance of about 238 μm marked as A, B, and C in Figure 2(a) was sliced. This distance is approximately equal to the primary dendrite arm spacing. The corresponding dendritic structure of the three sections is shown in Figures 2(b) through (d). Surface to the left is the sample surface. M stands for matrix and S is sliver. In Figure 2(b) (plane A), the tertiary branches developed from the secondary arm at the diverging boundary between the mold wall and matrix were observed. Some of the tertiary branches continued to grow into new primary dendrites. One of them was physically blocked by the neighboring dendrites (marked by the arrow). All dendrites were parallel to each other, *i.e.*, no misorientation generated in this plane. Tertiary branches developed from the secondary arm were also observed in Figure 2(c) (plane B). However, dendrites 2 and 5 obviously tilted from other dendrites and established misorientation from the matrix (dendrites 1, 3, and 4). It seems that dendrite 2 was blocked by dendrite 3 as marked by the arrow, but dendrite 5 grew continually at the diverging boundary without any restriction. Sliver arose from this deformed dendrite. In Figure 2(d) (plane C), dendrite arms grew in parallel and there was no misorientation in this plane. The XCT results indicate that sliver developed from only one row of the deformed dendrites at the diverging boundary. Furthermore, it was obtained in the XCT experiments that all of the slivers in nine castings originated from the diverging boundary between the matrix and mold wall.

The optical micrograph and EBSD results roughly corresponding to plane B in Figure 2(c) are shown in Figure 3. In Figure 3(a), the dendrites 1-5 corresponded to the dendrites 1-5 in Figure 2(c) and the finer tertiary branches that were difficult to be distinguished in XCT image can be observed. EBSD results shown in Figures 3(b) through (d) revealed the misorientation. Dendrite 5 and some fine tertiary branches around, as well as dendrite 2 were misaligned from matrix. This is in good agreement with the observation of XCT. These results further indicate that dendrites 2 and 5 not only tilted but also rotated from other dendrites, which resulted in a misorientation composed of both bending (Figure 3(c)) and torsion (Figure 3(d)). Figure 3(e) reveals the corresponding band contrast map. The quality of Kikuchi bands has been related to strain in previous publications.[23–27] The quality of Kikuchi bands is described by band contrast (BC, obtained using Oxford HKL Channel 5 software)[28] or pattern quality (PQ, obtained using EDAX TSL-OIM software).[29] High strain level (*i.e.*, dislocation density) results in low PQ or BC value.[29,30] Therefore, BC/PQ offers a qualitative measurement of deformation in the crystal.[28,31,32] Within the detected area I in Figure 3(a), the band contrast map illustrates that small local strain distributed homogenously within dendrite 5 and the surrounding fine tertiary dendrites, as well as the secondary dendrite on which they grew. However, the strain was only seen in the lower part of dendrite 5. No strain was detected as dendrite 5 grew upward (area II in Figure 3(a)). Small strain exhibited along the dendritic boundary also gradually disappeared. It is interesting to note that further growth of dendrites 2 and fine tertiary dendrites around dendrite 5 was suppressed by other dendrites. Only dendrite 5 with well-developed branches and near the casting surface survived. On the up left corner of Figure 3(a), another primary dendrite with same orientation of the matrix appeared (marked by the arrow). It probably developed from another dendrite in plane A or C (Figure 2).

The present experimental observations clearly demonstrate that sliver generally initiates as a result of dendrite branching and deformation at the diverging boundary. Branching occurs frequently when primary dendrite stems deviating from DS direction or there is geometry change in cross section of the casting.[6,33] The misorientation in a SX blade has been proposed as an inheritance of the mosaic structure in the secondary dendrite arms[34] or strain effect of γ' precipitation.[12] However, the strain distribution map shown in Figure 3(e) excludes these mechanisms as the strain neither localized in the secondary arm, nor distributed throughout the whole dendrite. Similarly, if bending of secondary arms due to buoyancy occurs, the deformation would concentrate only around the necking area

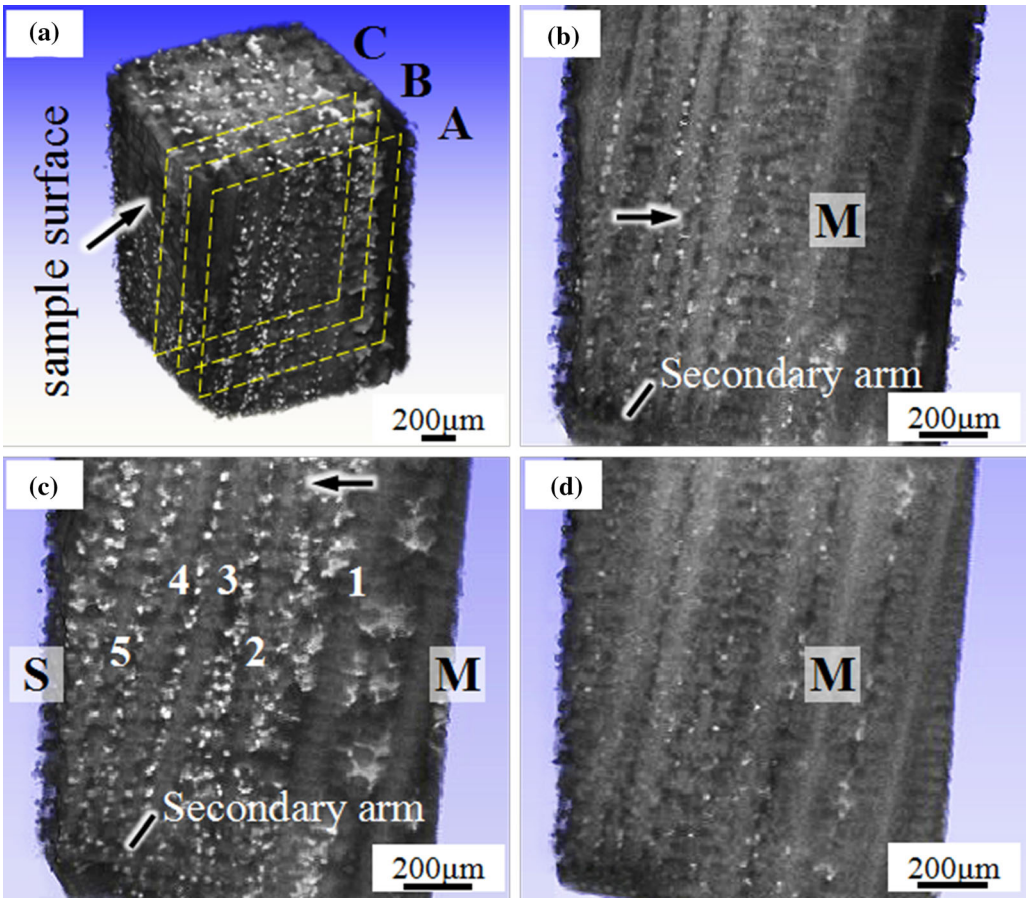

Fig. 2—XCT results of sliver. (*a*) The three-dimensional morphology of the sample. (*b*) through (*d*) Dendritic structures in plane A, B and C.

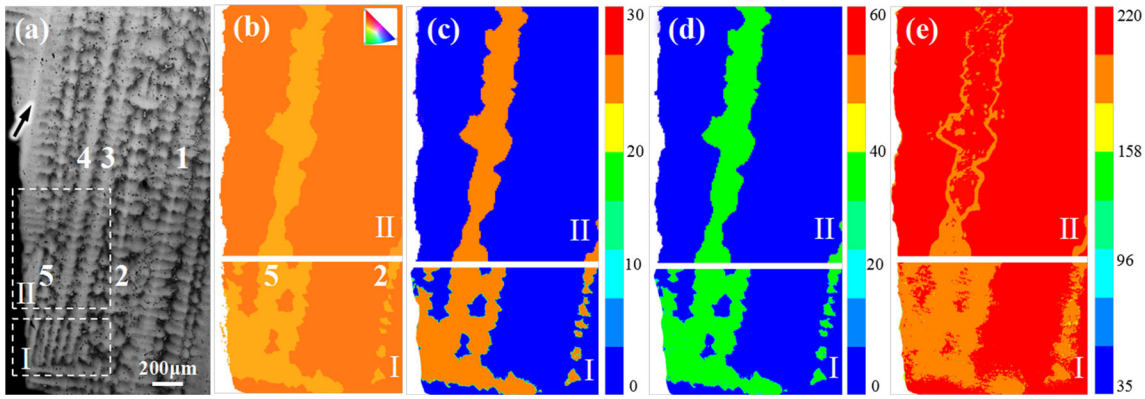

Fig. 3—(*a*) Optical micrograph of plane B in Fig. 2(c) and the corresponding (*b*) orientation map (contrasted by color of inverse pole figure inserted in the image), (*c*) bending and (*d*) torsion angle calculated with the EBSD data, and (*e*) band contrast map. EBSD maps shown in (b) through (e) are corresponding to the two rectangles labeled in (a) (Color figure online).

where the secondary arm connecting to the primary trunk. It is obvious that the deformation observed in the lower part of dendrite 5 and the surrounding tertiary dendrites, as well as the secondary dendrite arm on which they grew induced the sliver defect according to Figures 2 and 3. Besides, one can also confirm that the deformation occurs in the mushy zone. The free growth of the dendrite proceeded after deformation, which leads to the strain free dendrite in the upper part of the sliver. It is well known that plastic deformation in the mushy zone requires: (a) generation and (b) transmission of the stresses within the bridged dendrites as well as (c) sufficient ductility of the dendrites to allow bending or torsion.[7,33] The effect of interdendritic fluid flow in a single crystal superalloy has been studied in terms of permeability.[35] The permeability (velocity of

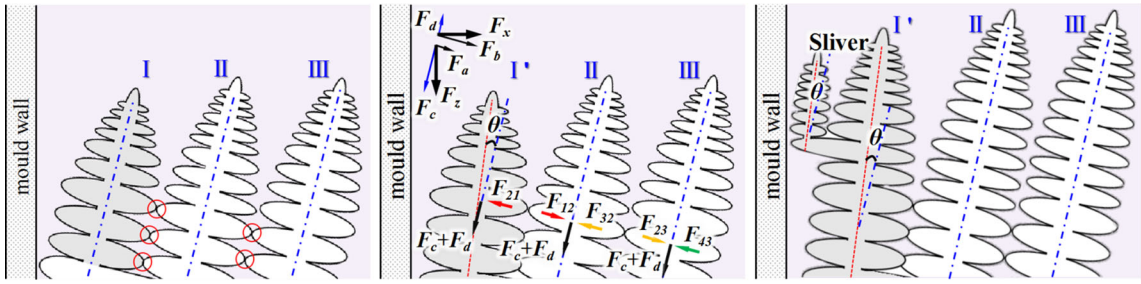

Fig. 4—Schematic illustration of the formation mechanism of sliver defect. (*a*) Development of new dendrite near the mold wall and establishment of dendrite bridging, (*b*) dendrite deformation induced by the unbalanced force arising from thermal contraction and (*c*) sliver formed as a result of the growing of deformed dendrite.

interdendritic fluid) becomes very low when the solid fraction $f_s > 0.6$. Moreover, the velocity in cross flow that would have been the main inducement for dendrite deformation is much smaller compared to that in the vertical direction. It has been well established that the bridging of dendrites only occurs at a relatively high solid fraction. For example, a f_s of > 0.7 was defined as the maximum packing solid fraction, below which dendrites deformation would not occur.[36] Hence, it is reasonable to deduce that interdendritic fluid flow that would have been a very important factor for freckle formation has little contribute to the formation of sliver defect. On the other hand, it can be confirmed that thermal contraction forces generated during solidification play an important role.

The formation mechanism of the sliver defect induced by thermal contraction is schematically illustrated in Figure 4. As shown in Figure 4(a), three tertiary dendrite arms (I, II and III) are growing from a secondary dendrite in the mushy zone due to the change in casting geometry or orientation deviation of a primary stem from the DS direction, and the dendrite bridging is built up (as marked by the red circles). Meanwhile, thermal contraction induces the downward (F_z) and inward (F_x) forces in the mushy zone as a result of geometrical constrain of the ceramic mold as exhibited in Figure 4(b). The forces loaded on the solidified dendrites (F_z and F_x) can be resolved into the forces along the dendrite axis (F_c and F_d) and perpendicular to the dendrite axis (F_a and F_b), respectively. It can be seen that a relative downward motion of the dendrites along the dendrite axis will occur due to the forces $F_c + F_d$, while the forces $F_a + F_b$ are transmitted between the bridged dendrites. The dendrite II is acted upon by the forces F_{12} and F_{32} arising from dendrite I and III and will not experience deformation because of the balanced forces. The dendrite III is acted upon by the balanced forces F_{23} and F_{43} arising from dendrite II and IV (not drawn in the Figure 4(b)) and there is also no deformation within it. However, the lower part of the dendrite I near the mold wall is therefore very likely to experience the mechanical deformation since the force F_{21} ($F_{21} = F_{21} = F_a + F_b$) applied by its neighbor dendrite II cannot be balanced, *i.e.*, the misorientation θ generates between dendrite I′ and II (or III). There is no bridging of the secondary dendrite arms on the upper part, and therefore no deformation is expected. Figure 4(c) shows that the later growth of dendrite I′ inherits the misorientation θ, but without strain. The deformed dendrite I′ continues to grow and branch at the diverging boundary and sliver defect forms finally. It is reasonable to believe that only those dendrites with well-developed branches (more bridging and therefore stress transmission) at the diverging boundary may evolve into sliver.

It is obvious that a better aligned [001] axis of the dendrites with less branching will have low possibility to generate slivers. Reduction of thermal contraction force, for example, by modification of mold materials and processing is also important. Moreover, any strategy that may increase the resistance of the mushy zone to deformation would be helpful, for instance, to reduce the length of the mushy zone to achieve a stronger dendritic skeleton.

In summary, the formation mechanism of sliver defect in Ni-based single crystal superalloy was investigated by XCT and EBSD. The following conclusions are drawn:

1. It was found that the diverging boundary between the primary dendrite arms and mold wall was the favorite position for the initiation of sliver. Sliver generated from 1 to 2 tertiary dendrites near the casting surface.
2. The deformation that induced sliver occurred in the mushy zone and was limited in the lower part of the dendrite. The free growth of the dendrite proceeded after deformation, which led to the strain free dendrite in the upper part of the sliver.
3. Compared to the interdendritic fluid flow, thermal contraction forces played an important role in the formation of sliver. The mechanical deformation that primarily occurred on a diverging boundary can be attributed to the imbalanced force loaded on the dendrite.

This work was financially supported by the National Natural Science Foundation of China (Grant Nos: 51631008, 91860201, 51771204, and U1732131) and National Science and Technology Major Project

(Grand No. 2017-VII-0008-0101). The authors are grateful for those supports.

REFERENCES

1. R.C. Reed: *The Superalloys: Fundamentals and Applications*, Cambridge University Press, Cambridge, 2006.
2. T.M. Pollock and S. Tin: *J. Propul. Power*, 2006, vol. 22, pp. 361–74.
3. N. Stanford, A. Djakovic, B.A. Shollock, M. McLean, N. D'Souza, and P.A. Jennings: *Scripta Mater.*, 2004, vol. 50, pp. 159–63.
4. S. Tin, T.M. Pollock, and W. Murphy: *Metall. Mater. Trans. A*, 2001, vol. 32A, pp. 1743–53.
5. A. Morawiec: *Scripta Mater.*, 2009, vol. 61, pp. 438–40.
6. D.J. Sun, L. Liu, T.W. Huang, W.C. Yang, C. He, Z.R. Li, J. Zhang, and H.Z. Fu: *Metall. Mater. Trans. A*, 2019, vol. 50A, pp. 1119–24.
7. J.W. Aveson, P.A. Tennant, B.J. Foss, B.A. Shollock, H.J. Stone, and N. D'Souza: *Acta Mater.*, 2013, vol. 61, pp. 5162–71.
8. Z.X. Shi, S.Z. Liu, and J.R. Li: *Hot Work. Technol.*, 2013, vol. 42, pp. 31–37.
9. R.D. Doherdy: *Scripta Mater.*, 2003, vol. 49, pp. 1219–22.
10. G. Reinhart, H. Nguyen-Thi, N. Mangelinck-Noël, J. Baruchel, and B. Billia: *JOM*, 2014, vol. 66, pp. 1408–14.
11. J.W. Aveson, G. Reinhart, H. Nguyen-Thi, N. Mangelinck-Noël, A. Tandjaoui, B. Billia, K. Goodwin, T.A. Lafford, J. Baruchel, H.J. Stone, and N. D'Souza: *Superalloys 2012*, TMS, Warrendale, PA, 2012, pp. 615–24.
12. N. Siredey, M. Boufoussi, S. Denis, and J. Lacaze: *J. Cryst. Growth*, 1993, vol. 130, pp. 132–46.
13. S. Henry, T. Minghetti, and M. Rappaz: *Acta Mater.*, 1998, vol. 46, pp. 6431–43.
14. S. Tin and T.M. Pollock: *Mater. Trans. A*, 2003, vol. 34A, pp. 1953–67.
15. J. Pilling and A. Hellawell: *Metall. Mater. Trans. A*, 1996, vol. 27A, pp. 229–32.
16. D. Ruvalcaba, R.H. Mathiesen, D.G. Eskin, L. Arnberg, and L. Katgerman: *Acta Mater.*, 2007, vol. 55, pp. 4287–92.
17. R.H. Mathiesen, L. Arnberg, P. Bleuet, and A. Somogyi: *Metall. Mater. Trans. A*, 2006, vol. 37A, pp. 2515–24.
18. A.M. Mullis: *Mater. Sci. Eng. A*, 2001, vols. 304–306, pp. 245–49.
19. K. Dragnevski, A.M. Mullis, D.J. Walker, and R.F. Cochrane: *Acta Mater.*, 2002, vol. 50, pp. 3743–55.
20. S.S. Hu, L. Liu, W.C. Yang, D.J. Sun, M. Huo, T.W. Huang, J. Zhang, H.J. Su, and H.Z. Fu: *Metall. Mater. Trans. A*, 2019, vol. 50A, pp. 1607–10.
21. S.G. Wang, S.C. Wang, and L. Zhang: *Acta Metall. Sin.*, 2013, vol. 49, pp. 897–910.
22. L. Zhang and S.G. Wang: *Materials*, 2018, vol. 11, pp. 1795–1820.
23. P.N. Quested, P.J. Henderson, and M. Mc Lean: *Acta Metall.*, 1988, vol. 36, pp. 2743–52.
24. A.J. Wilkinson: *Mater. Sci. Eng. A*, 1991, vol. 135, pp. 189–93.
25. A.J. Wilkinson and D.J. Dingley: *Acta Metall. Mater.*, 1991, vol. 39, pp. 3047–55.
26. A.J. Wilkinson and D.J. Dingley: *Acta Metall. Mater.*, 1992, vol. 40, pp. 3357–68.
27. S. Mukherjee, H. Garmestani, and N. Chandra: *Scripta Metall. Mater.*, 1995, vol. 33, pp. 93–99.
28. M.P. Black and R.L. Higginson: *Scr. Mater.*, 1999, vol. 41, pp. 125–29.
29. A.W. Wilson, J.D. Madison, and G. Spanos: *Scripta Mater.*, 2001, vol. 45, pp. 1335–40.
30. R. Saha, R.K. Ray, and D. Bhattacharjee: *Scripta Mater.*, 2007, vol. 57, pp. 257–60.
31. J. Tarasiuk, Ph. Gerber, and B. Bacroix: *Acta Mater.*, 2002, vol. 50, pp. 1467–77.
32. F.J. Humphreys: *J. Mater. Sci.*, 2001, vol. 36, pp. 3833–54.
33. N. D'Souza, M. Newell, K. Devendra, P.A. Jennings, M.G. Ardakani, and B.A. Shollock: *Mater. Sci. Eng. A*, 2005, vols. 413–414, pp. 567–70.
34. W. Bogdanowicz, R. Albrecht, J. Sieniawski, and K. Kubiak: *J. Cryst. Growth*, 2014, vol. 401, pp. 418–22.
35. J. Madison, J. Spowart, D. Rowenhorst, L.K. Aagesen, K. Thornton, and T.M. Pollock: *Acta Mater.*, 2010, vol. 58, pp. 2864–75.
36. A.K. Dahle and D.H. StJohn: *Acta Mater.*, 1998, vol. 47, pp. 31–41.